Size effect on the ordering of $L1_0$ FePt nanoparticles

T. Miyazaki, O. Kitakami,* S. Okamoto, and Y. Shimada
Division of Advanced System, Institute of Multidisciplinary Research for Advanced Materials, Tohoku University, 2-1-1 Katahira, Sendai 980-8577, Japan

Z. Akase, Y. Murakami, and D. Shindo
Division of Materials Control, Institute of Multidisciplinary Research for Advanced Materials, Tohoku University, 2-1-1 Katahira, Sendai 980-8577, Japan

Y. K. Takahashi and K. Hono
National Institute for Materials Science, 1-2-1 Sengen, Tsukuba 305-0047, Japan
(Received 16 November 2004; revised manuscript received 11 August 2005; published 20 October 2005)

We have studied the size effect on the $L1_0$ ordering of FePt (001) nanoparticles epitaxially grown on MgO (001). From the dark field images using 110 superlattice spots excited by incident electron beam along $[\bar{1}1l]$ (l=4–6), the critical size for $L1_0$ ordering has been evaluated to be d=1.5–2 nm below which no ordering occurs. Further, we have taken an electron diffraction pattern of each FePt nanoparticle using a nanometer-sized electron beam and determined the respective long-range order parameter S by analyzing the superlattice/fundamental diffraction intensity ratio based on the multislice method. It is found that the order parameter S sharply drops below $d\sim3$ nm and decreases to zero for $d<2$ nm, the result is almost consistent with thermodynamic calculations previously reported. The present work unambiguously shows that the ordering of $L1_0$ FePt is entirely inhibited when its size is less than $d\sim2$ nm. Such size effect is not so serious for practical applications of FePt to permanent magnets or magnetic recording media because the effect is significant only for $d<2$ nm where the $L1_0$ FePt would be magnetically unstable due to severe thermal agitation.

DOI: 10.1103/PhysRevB.72.144419 PACS number(s): 81.07.Bc, 85.70.Kh, 64.70.Kb, 64.60.Cn

Equiatomic FePt forms a chemically ordered $L1_0$ structure below 1300 °C, where there are alternating atomic planes of Fe and Pt along the c axis,[1] resulting in a tetragonal distortion in the unit cell and extremely large magnetic anisotropy energy of 7×10^7 erg/cc.[2] $L1_0$ FePt is expected to exhibit excellent hard magnetic properties even when its size is as small as 3 to 4 nm, due to its large magnetic anisotropy. Therefore much attention has been placed on fabrication and magnetic properties of nanostructured $L1_0$ FePt both from scientific and technological interests. Especially self-assembled monodisperse FePt nanoparticles are of particular interest for future ultrahigh density heat-assisted magnetic recording.[3,4] Recently a few studies have reported that equiatomic FePt is not transformed into the equilibrium $L1_0$ order phase when its size is less than several nanometers.[5–12] For example, Takahashi *et al.*[5] evaluated the long-range order parameter S of FePt granular films and found that the critical size for ordering was $d\sim3$ nm, being somewhat larger than the thermodynamic calculation using optimized nearest-neighbor Lennard-Jones potentials. A very similar critical size has been reported in thermodynamic calculations[9] and Monte Carlo simulations[11] based on the regular lattice Ising model.[13] Such instability of the order phase is mainly due to loss of bonding energy at the surface sites, in addition to other surface effects.[11,14] In the previous experiment on FePt-Al_2O_3 granular films,[5,6] the order parameter S was determined from the electron diffraction intensity ratio I_{110}/I_{111} under the assumption of the kinematical diffraction theory, where I_{110} and I_{111} are the intensity for superlattice 110 and fundamental 111 diffractions, respectively. Furthermore, the size effect was discussed based on the mean particle size d_m in spite of the nontrivial size distribution.

In the present work, we investigate the size effect on the ordering of $L1_0$ FePt (001) epitaxial particles. From the dark field images using superlattice 110 spots, we clarify the critical size for the ordering. Furthermore, we determine the order parameter S of each FePt naoparticle from its diffraction pattern taken by nanometer-sized electron beam, and clarify the relationship between the particle size d and the parameter S.

FePt nanoparticles were directly grown on MgO(001) by sputtering a Fe-50 at. % Pt target. The composition of the particles was found to be Fe-42 at. % Pt by the energy dispersive x-ray fluorescence spectroscopy. The substrate temperature and the Kr gas pressure during sputtering were, respectively, fixed at 973 K and 30 mTorr, yielding highly ordered epitaxial $L1_0$ FePt (001) without any crystal domain variants, as has been reported in previous papers.[15,16] In this study, the nominal deposition thickness of FePt was t_n =1–10 nm, which is an equivalent amount of FePt if it is a continuous film. The x-ray diffractometry (XRD) confirmed epitaxial growth of $L1_0$ FePt (001) with excellent c-axis orientation of $\Delta\theta_{50}$=1.2° (~20 mrad). The particle shape was checked by plan-view and cross-sectional TEM images. For a very thin thickness range of $t_n<3$ nm, each particle was well isolated from each other and identified as an oblate spheroid with the aspect ratio (height/diameter)=0.5–1.0. The order parameter S was evaluated by electron diffractometry (ED) along with XRD using synchrotron radiation with the wavelength of 0.116 nm. After cooling the sample, car-

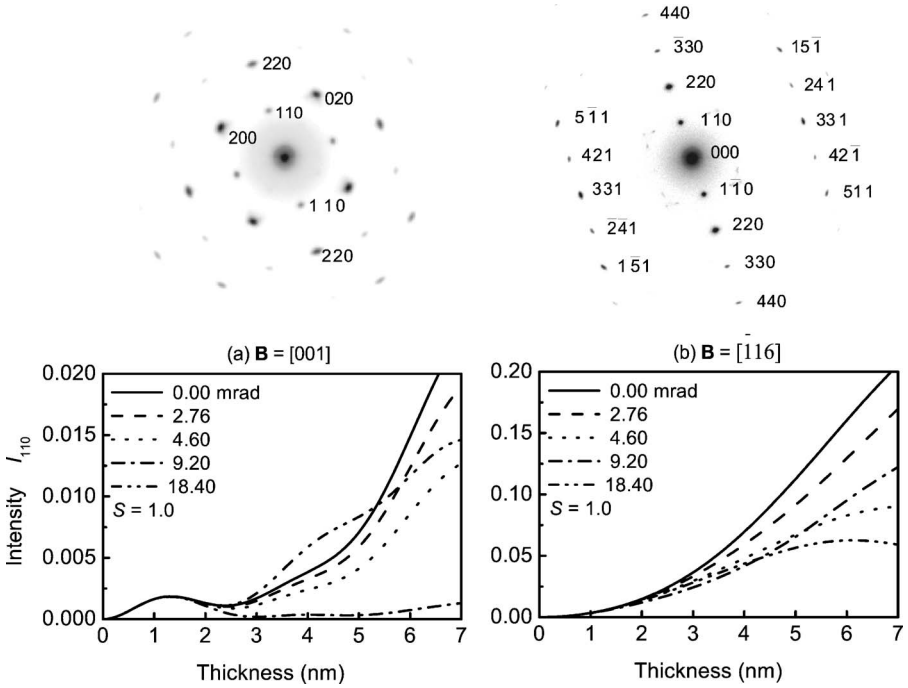

FIG. 1. Calculated diffraction intensity I_{110} for incident beam with (a) $\mathbf{B}=[001]$ and (b) $[\bar{1}16]$ as functions of FePt thickness for various deviation angles toward $[\bar{1}10]$ from the respective zone axes. The upper two panels show the typical SAED patterns of $L1_0$ FePt (001) obtained with $\mathbf{B}=[001]$ (left) and $[\bar{1}16]$ (right).

bon was deposited as a capping and supporting layer for TEM observations. Thin foils for TEM observations were prepared by the following chemical etching process instead of the conventional ion milling method, because Ar^+ ions with acceleration energy of 3 keV severely destroyed the $L1_0$ structure. We found that a FePt layer covered with a C supporting layer was easily detached from a MgO substrate by immersing it into a solution containing phosphoric (98 vol %) and sulfuric (2 vol %) acids at temperatures of $T=310-375$ °C for 1 h. Even after etching the sample with $t_n=4$ nm for 10 h, no change was found in the sample morphology as checked by SEM and TEM, the crystal structure and order parameter S by XRD and ED, and total magnetic moments by a vibrating sample magnetometer. Prior to electron diffraction experiments, accurate adjustment of the zone axis $L1_0$ FePt [001] was carried out by monitoring Kikuchi patterns. After very careful zone axis adjustment for each particle, the corresponding diffraction pattern was taken with incident electron beam along $\mathbf{B}=[\bar{1}16]$ in order to excite $hh0$ systematic reflections. In general, electron diffraction intensity is considerably influenced by the sample thickness and misalignment of the zone axis due to very complicated multiple electron scattering events in solids. However, the intensity behavior becomes very simple when selective excitation of the systematic reflections mentioned above is adopted. We calculated diffraction intensities I_{110}, I_{220} and their ratio I_{110}/I_{220} by means of the multislice method[17] to take dynamical diffraction effects into account. Figures 1(a) and 1(b), respectively, show the calculated diffraction intensity I_{110} for incident beam with $\mathbf{B}=[001]$ and $[\bar{1}16]$ as functions of the FePt thickness for various deviation angles toward $[\bar{1}10]$ from the respective zone axes, along with typical corresponding SAED (selected area electron diffraction) patterns from the 2-nm-thick $L1_0$ FePt (001). Here the diffraction intensity is normalized by the incident beam strength. Note in Fig. 1(a) that the intensity behaves in a very complicated manner depending on very slight misalignment of incident beam and thickness. In contrast, the situation becomes quite simple[7,18] and the intensity is greatly enhanced when the $hh0$ systematic reflections are selectively excited by incident beam along $\mathbf{B}=[\bar{1}16]$, as shown in Fig. 1(b). Figure 2 shows the bright field (BF) images and the corresponding dark field (DF) images using $L1_0$ FePt 110 superlattice spots taken with (a) $\mathbf{B}=[001]$ and (b) $[\bar{1}16]$ for the FePt ($t_n=2$ nm) sample with the average order parameter S of 0.83. Note that

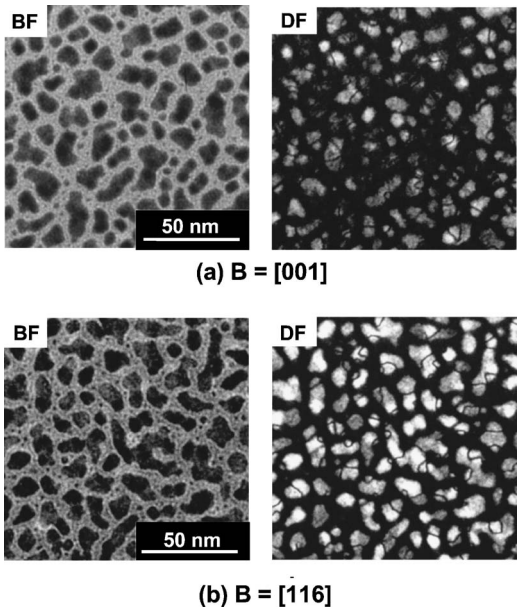

FIG. 2. Bright field (BF) and the corresponding dark field (DF) images using $L1_0$ FePt 110 superlattice spots taken with (a) $\mathbf{B}=[001]$ and (b) $[\bar{1}16]$ for the FePt ($t_n=2$ nm) sample with the average order parameter S of 0.83.

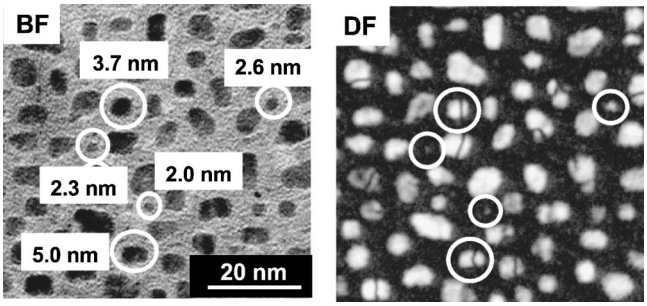

FIG. 3. Bright field (BF) and the corresponding dark field (DF) images using $L1_0$ FePt 110 superlattice spots taken with $\mathbf{B}=[\bar{1}16]$ for the FePt ($t_n=1$ nm) sample with the average order parameter S of 0.80. Note that antiphase boundaries (APB) can be clearly observed in somewhat larger particles.

all $L1_0$ FePt (001) particles are visible in the DF image for $\mathbf{B}=[\bar{1}16]$, as shown in Fig. 2(d), while a large number of particles remain dark for $\mathbf{B}=[001]$ [Fig. 2(b)] mainly due to very weak diffraction intensity and/or slight deviation of incident beam direction $\mathbf{B}$ with respect to the zone axis. Figure 3 shows the BF and DF images using a 110 superlattice spot taken with $\mathbf{B}=[\bar{1}16]$ for the FePt sample with the nominal thickness $t_n=1$ nm. We note that $L1_0$ ordering occurs even for very small size of $d\sim 2$ nm. In addition, we can clearly observe antiphase boundaries (APB) in somewhat larger particles, which are probably introduced by coalescense of nucleated islands during thin film growth process. We observed a lot of DF images and counted the number of ordered ($S>0$) and disordered ($S=0$) particles. As shown in Fig. 4, $L1_0$ ordering is entirely inhibited for $d<2$ nm. Let us discuss whether the above size effect is crucial for practical applications of $L1_0$ FePt nanoparticles from the standpoint of magnetic thermal stability. For an isolated nanoparticle with two energy minima, the probability per unit time of successfully crossing the barrier is given by $1/\tau=f_0\exp(-\Delta E/k_BT)$, where τ is the relaxation time for magnetization reversal, f_0 is the attempt frequency which is of the order of 10^{10} Hz for $L1_0$ FePt nanoparticles,[15] ΔE is the height of the energy barrier for magnetization reversal which is nearly equal to $K_u\nu$ (K_u: magnetic anisotropy energy per unit volume, ν: particle volume) for an isolated Stoner-Wohlfarth type magnet, k_B is the Boltzmann constant, and T is the temperature. If the relaxation time of 10 years is required for long-term data storage, the barrier $\Delta E/k_BT$ should be larger than 42.5. Assuming an ideally spherical $L1_0$ FePt particle with the anisotropy energy of $K_u=7\times10^7$ erg/cc,[2] the critical diameter d_{cr} for thermal stability must be larger than 3.5 nm. Since the above critical size of about 2 nm for $L1_0$ ordering is much smaller than that for magnetic thermal stability, the size effect on $L1_0$ ordering would be not so crucial for practical applications if one can accurately control the size of FePt nanoparticles with negligibly small size distribution. Figure 4 also plots the frequency of FePt nanoparticles containing APB. The frequency remains zero up to $d<4$ nm and then begins to increase very rapidly, suggesting that the maximum nucleated island size before coalescense is roughly $d\sim 4$ nm. It is easily anticipated that the boundary size for APB to appear will decrease on decreasing the growth temperature because of reduced surface diffusion of adatoms during thin film growth process. In fact, we recently confirmed that the boundary size for APB to appear decreased with decreasing the growth temperature of FePt films.[19] Considering that magnetic anisotropy could be degraded at APB due to local symmetry breaking of $L1_0$ anisotropic atomic configuration, it is favorable to reduce APB in order to keep hard magnetic properties of FePt nanoparticles. Growth at a higher temperature would be very effective for this purpose.

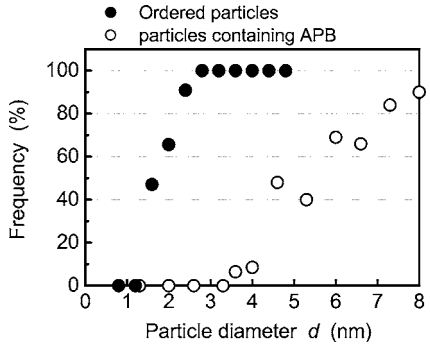

FIG. 4. Frequency of $L1_0$ FePt (001) ordered particles (solid circles) and of FePt particles containing APB (empty circles) as functions of particle diameter. The data were obtained from several samples with the nominal thickness of $t_n=1$ nm.

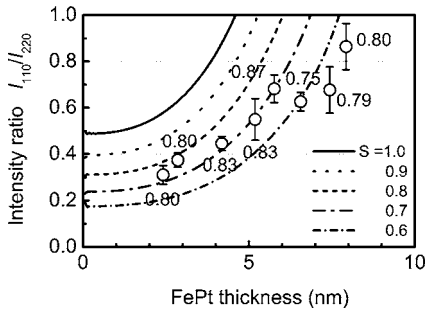

FIG. 5. Intensity ratio I_{110}/I_{220} measured from the SAED patterns for incident beam with $\mathbf{B}=[\bar{1}16]$ as a function of the FePt thickness. The lines show the intensity ratio for various S calculated by the multislice method for $\mathbf{B}=[\bar{1}16]$, and the numbers near the data points indicate the order parameter S determined by XRD using synchrotron radiation.

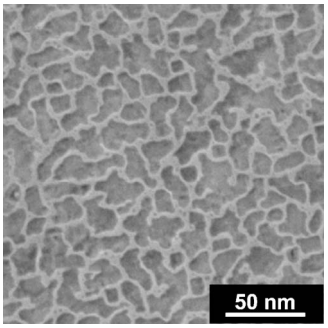

FIG. 6. In-plane bright field image of the FePt sample with the nominal thickness of $t_n=4$ nm.

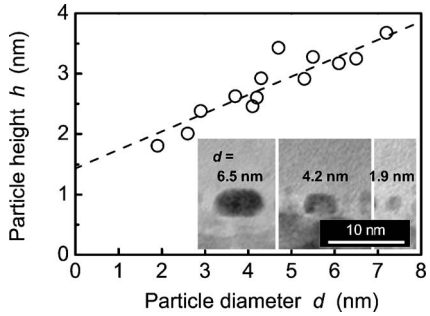

FIG. 7. Height h of FePt particles as a function of the particles diameter d. The inset shows the cross sectional TEM image. The data were obtained from several samples with the nominal thickness of $t_n=1$ nm.

In Fig. 5, the intensity ratio I_{110}/I_{220} measured from the SAED patterns of various FePt samples are plotted as a function of the nominal film thickness t_n above 3 nm. For $t_n \gtrsim 3$ nm, FePt grows laterally and forms densely packed flat islands as shown in Fig. 6, so that it is appropriate to approximate it as a uniform thin film. The lines in the figure show the intensity ratio for various S calculated by the multislice method to take the dynamical diffraction effect into account. The numbers near the data points indicate the order parameter S determined by XRD using synchrotron radiation. Note that the multislice calculations well reproduce the values determined by XRD, indicating that the multislice method is appropriate for calculation of electron diffraction intensity.

So far the size effect on the ordering of $L1_0$ FePt nanoparticles has been discussed based on the mean particle size in spite of large particle size distribution. For more quantitative and reliable discussions, we have to evaluate the order parameter S for each $L1_0$ FePt particle with well-characterized diameter and height. From cross-sectional TEM observations, we measured the particle diameter d and height h of each FePt particle, as shown in Fig. 7. For the range of $h=2.0-3.5$ nm in Fig. 7, we calculated electron diffraction intensity I_{110} and I_{220} for $\mathbf{B}=[\bar{1}16]$ based on the multislice method. In Fig. 8, the ratio I_{110}/I_{220} is plotted as functions of the order parameter S for various particle height h. Using this result, we can evaluate the order parameter S of each $L1_0$ FePt nanoparticle from experimentally determined

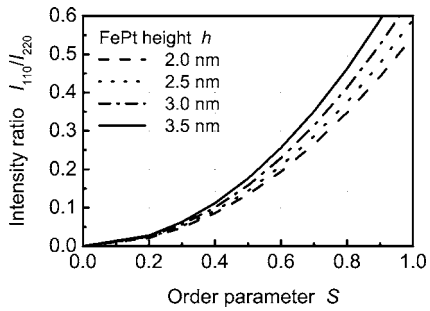

FIG. 8. Calculated intensity ratio I_{110}/I_{220} for incident beam with $\mathbf{B}=[\bar{1}16]$ based on the multislice method as a function of the order parameter S for various particle height h.

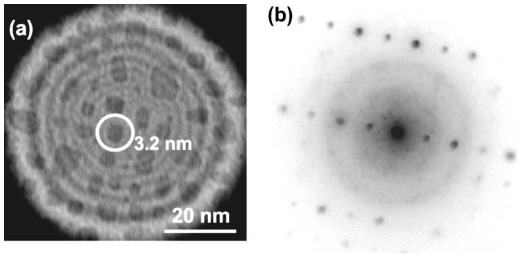

FIG. 9. Typical example of the nanobeam electron diffraction pattern (b) for incident beam with $\mathbf{B}=[\bar{1}16]$ from the particles ($d=3.2$ nm) encircled in (a).

I_{110}/I_{200}. In order to determine the order parameter S of each particle, we carried out an electron diffraction experiment using a focused electron beam with the diameter of ~ 1 nm. For each particle, after very careful adjustment of the zone axis by monitoring its Kikuchi pattern, we recorded its diffraction pattern onto an imaging plate with excellent linear response to incoming electrons, and then measured the diffraction intensity ratio I_{110}/I_{220}. Figure 9(b) shows the typical example of the electron diffraction pattern from the particle ($d=3.2$ nm) encircled in Fig. 9(a). We have carried out these elaborate measurements for 24 particles and investigated the relationship between the order parameter S and particle diameter d. The result is shown in Fig. 10. We note that the order parameter S sharply drops below $d \sim 3$ nm and decreases to zero for $d<2$ nm, the result is almost consistent with the thermodynamic calculations previously reported.[5,8,9,11] The present work unambiguously shows that the ordering of $L1_0$ FePt is entirely inhibited when its size is below $d \sim 2$ nm.

In summary, the size effect on the ordering of $L1_0$ FePt nanoparticles was investigated. We obtained electron diffraction patterns from each nanoparticle using a nanometer-sized electron beam along $[\bar{1}16]$ and determined the respective long-range order parameter S by analyzing the superlattice/fundamental diffraction intensity ratio based on the multislice method. It was found that the long range order parameter S sharply dropped below $d \sim 3$ nm and decreased to zero for $d<2$ nm. This result unambiguously indicated that the

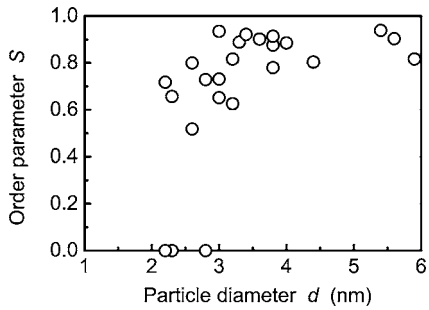

FIG. 10. Relationship between the order parameter S and particle diameter d. The data were obtained from several samples with the nominal thickness of $t_n=1$ nm.

$L1_0$ ordering of FePt was entirely inhibited when its size was smaller than $d \sim 2$ nm. Nevertheless, this size effect seemed not to be so serious for practical applications because the effect is significant only for the size where $L1_0$ FePt particles became superparamagnetic at room temperature.

One of the authors (T.M.) greatly acknowledges financial support from a SRC scholarship. We would like to express sincere thanks to Professor Y. Hirotsu and K. Sato at Osaka University for their fruitful discussions and useful information. The present work was supported by the Grants-in-Aid of the Japan Society for the Promotion of Science, the Special Coordination Funds for Promoting Science and Technology on "Nanohetero Metallic Materials" from the Ministry of Education, Culture, Sport, Science and Technology, the IT21-program (RR2002) of MEXT, and the Storage Research Consortium in Japan.

*Corresponding author. Email address: kitakami@tagen.tohoku.ac.jp

[1] M. Hansen, *Constitution of Binary Alloys* (McGraw-Hill, New York, 1958).
[2] O. A. Ivanov, L. V. Solina, V. A. Demshina, and L. M. Magat, Phys. Met. Metallogr. **35**, 92 (1973).
[3] S. Sun, C. B. Murray, D. Weller, L. Folks, and A. Moser, Science **287**, 1989 (2000).
[4] S. Sun, D. Weller, and C. Murray, in *The Physics of Ultra-High-Density Magnetic Recording*, edited by M. L. Plumer, J. v. Ek, and D. Weller (Springer, New York, 2001), pp. 249–276.
[5] Y. K. Takahashi, T. Ohkubo, M. Ohnuma, and K. Hono, J. Appl. Phys. **93**, 7166 (2003).
[6] Y. K. Takahashi, T. Koyama, M. Ohnuma, T. Ohkubo, and K. Hono, J. Appl. Phys. **95**, 2690 (2004).
[7] K. Sato and H. Hirotsu, Mater. Trans., JIM **44**, 1523 (2003).
[8] T. Koyama and H. Onodera, Mater. Trans., JIM **44**, 1518 (2003).
[9] S. Fukami and N. Tanaka, Philos. Mag. Lett. **84**, 33 (2004).
[10] T. Saito, O. Kitakami, and Y. Shimada, J. Magn. Magn. Mater. **239**, 310 (2002).
[11] B. Yang, M. Asta, O. N. Mryasov, T. Klemmer, and R. W. Chantrell, Scr. Mater. **53**, 417 (2005).
[12] S. Fukami, A. Ohno, and N. Tanaka, Mater. Trans., JIM **45**, 2012 (2004).
[13] C. Mottet, G. Treglia, and B. Legrand, Phys. Rev. B **66**, 045413 (2002).
[14] M. Kozowski, R. Kozubski, V. Pierron-Bohnes, and W. Pfeiler, Comput. Mater. Sci. **33**, 287 (2005).
[15] S. Okamoto, O. Kitakami, N. Kikuchi, T. Miyazaki, Y. Shimada, and Y. K. Takahashi, Phys. Rev. B **67**, 094422 (2003).
[16] S. Okamoto, N. Kikuchi, O. Kitakami, T. Miyazaki, Y. Shimada, and K. Fukamichi, Phys. Rev. B **66**, 024413 (2002).
[17] J. M. Cowley, *Diffraction Physics*, 2nd ed. (North-Holland, Amsterdam, 1981), pp. 225–247.
[18] K. Sato, Y. Hirotsu, H. Mori, Z. Wang, and T. Hirayama, J. Appl. Phys. **97**, 084301 (2005).
[19] T. Miyazaki, S. Okamoto, O. Kitakami, Y. Shimada, Z. Akase, Y. Murakami, D. Shindo, Y. K. Takahashi, and K. Hono, presented at Intermag 2005, Nagoya, Japan.